Chapter-5

Hybrid inorganic-organic inverted solar cells with ZnO/ZnMgO barrier layer and effective organic active layer for low leakage current, enhanced efficiency, and reliability

CHAPTER CONTENT

5.1. Introduction:

Organic solar cells (OSCs) and organic photovoltaics (OPVs) have attracted considerable interest in clean energy research. This is because they can be prepared at low cost, and are lightweight alternatives to the currently used single-junction wafer-based silicon solar cells [268]. From the standpoint of making these devices industry-relevant, improvements in the device structure, as well as performance, are essential. In general, optimization of device architecture can pave the way for addressing efficiency losses, which are very common due to the presence of defect states [269] in the heterostructure. Also, efficiency enhancement may be pursued through the use of low bandgap polymers. The mere use of the right materials is insufficient to achieve better cell performance unless they form optimum cell architecture. The materials processes involved in the deployment of these polymers need to be carefully explored as well. Currently, through careful fabrication approaches in layered structures, OSCs with good efficiencies have been realized [270,271], however, they have some reliability issues. So, the challenges continue to exist, from both the processing and device architecture stand points.

In the bulk-heterojunction (BHJ) architecture, which has a distinct advantage from a processing standpoint, efficiencies are less reliable due to environmental degradations. BHJ devices usually have lower device stability and are highly air-sensitive [272]. In OPVs, the interface between organic and inorganic counterparts plays a crucial role, too. These interfaces are often considered the first place where losses and degradations occur. Hence, interfacial engineering is an essential approach for addressing some of the contemporary challenges associated with OPVs [273-275].

Due to the above considerations, improving the performance of hybrid photovoltaic devices (HPD) through the engineering of the inorganic/organic material interfaces has

become relevant [276]. As a replacement for the conventional device structure, stable inverted-type OSCs (which utilize metal oxides and are also known as IOSCs) have gained significant attention among researchers [277-279]. For efficient electron collection, inorganic electron-selective layers like cesium carbonate (Cs2O3) [280], titanium dioxide (TiO2) [281], calcium (Ca) [282], titanium chelate (TIPD) [283] and ZnO [284] are used in IOSCs.

From the device architecture standpoint, the materials should be so chosen that oxygen diffusion is reduced; because oxygen diffusion can directly result in cell degradation. Typically, diffusion of oxygen into the active layer occurs through pinholes and also due to the corrosion of the indium tin oxide (ITO) electrode. This is primarily due to the acidic and hygroscopic nature of PEDOT:PSS [poly(3,4-ethylene dioxythiophene):poly(styrenesulfonate)] [285,286]. Hence, the introduction of a suitable barrier layer (mainly metal oxide) over the ITO electrode is reasonable. It is worth mentioning that, along with minimizing the oxygen diffusion and defect states, optimizing both shunt and series resistances as well as the short circuit current density is a known challenge for fabricating good quality organic solar cells. The present work makes a modest attempt to achieve the above goal by the use of ZnO/ZnMgO bilayer that helps in better electron collection as well as serves as a substantial barrier layer. The inverted OSC demonstrated here showed good nature of external quantum efficiency, and overall photoconversion efficiency was ~4.95%. The detailed structural, optical, and electrical characterizations of the synthesized layers have been carried out in this work.

5.2 Experimental Section

5.2.1. Material selection:

P3HT and PCBM (with 99.5% purity) were obtained from American Dye Source, Inc. PEDOT:PSS (Clevios PVP AI 4083) was purchased from Heraeus Inc. Commercially available (Merck) ITO coated glass substrates with sheet resistance of ~10 Ω/sq were used as base substrates. Zinc nitrate hexahydrate ($Zn(NO_3)_2 \cdot 6H_2O$, >98% purity) and hexamethylenetetramine ($C_6H_{12}N_4$) were procured from Sigma Aldrich and used without any further purification. 18 MΩ double distilled water and chlorobenzene (PhCl or C_6H_5Cl, 99.8%) were used to prepare the solutions. [Nomenclature: PCBM is [6,6]-phenyl-C_{61}-butyric acid methyl ester, P_3HT is poly(3-hexylthiophene),PEDOT is poly(3,4-ethylene dioxythiophene) and PSS is poly(styrenesulfonate)].

5.2.2. Cell fabrication:

In this work, inverted OSCs (IOSCs) with and without incorporating ZnO/ZnMgO barrier layer and ZnO nanorod (NR) structures have been fabricated to have a comparative idea about their cell parameters. Cells with four different configurations have been fabricated with 0.3 cm × 0.3 cm active area. The layer-wise schematic presentations of the cells are shown in Fig.5.1 and can be expressed as follows:

- Cell A: ITO/PCBM/P3HT:PCBM/PEDOT:PSS/Ca-Al (all organic)
- Cell B: ITO/ZnONR/PCBM/P3HT:PCBM/PEDOT:PSS/Ca-Al
- Cell C: ITO/ZnO/ZnMgO/PCBM/P3HT:PCBM/PEDOT:PSS/Ca-Al
- Cell D: ITO/ZnO/ZnMgO/ZnONR/PCBM/P3HT:PCBM/PEDOT:PSS/Ca-Al

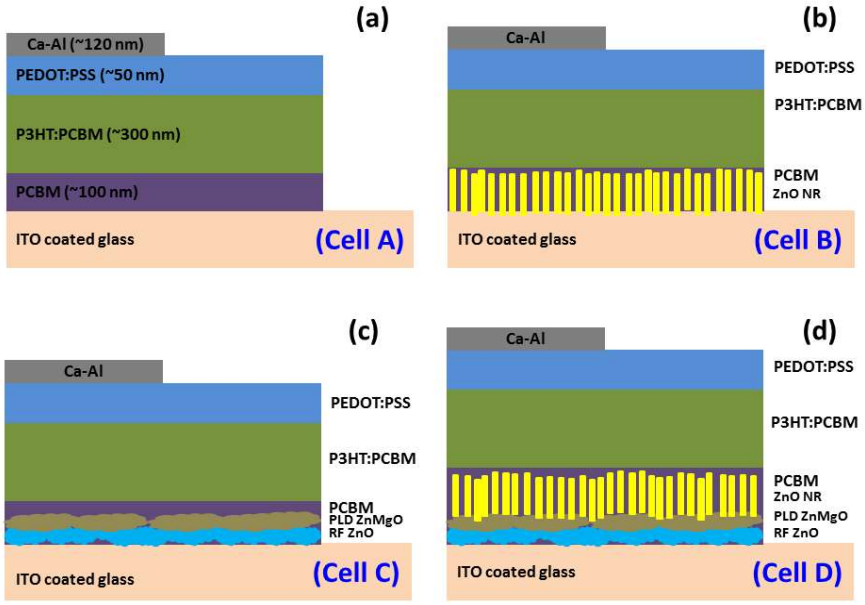

Fig.5.1. Schematic of the fabricated solar cells with different configurations.

The base substrate was indium tin oxide (ITO) coated glass in all the cases. The substrates were ultrasonically cleaned with acetone and ethanol and subsequently boiled in isopropanol. In all cases, the top contact was taken by e-beam evaporation (at 3×10^{-5}mBar) of Ca (~10 nm) and Al (~110 nm) layers through a shadow mask.

For Cell A, which is a purely organic cell, the compounds were deposited sequentially using the spin-coating technique on the cleaned ITO substrate. In this case, first, a carrier-selective layer of PCBM (~ 100 nm) was deposited on the ITO substrate by drop-wise adding 60 µL at an rpm of 1000 for 60 s. Next, instead of using only P3HT like the conventional cases, a blend (80 µL) of P3HT:PCBM with thickness ~ 300 nm was coated on it at 1200 rpm for 45 s. The mixture was prepared by mixing P3HT and PCBM at a 1:1 wt% ratio in chlorobenzene and stirring at 1400 rpm for 25 hr at 70°C. This is necessary to facilitate the carrier separation by increasing the field strength within this layer. As reported by Dang et al. [287] and Jin et al. [288], the performance of an OSC does not vary linearly with increasing P3HT:PCBM layer thickness. Therefore, the P3HT:PCBM layer, in this case, was chosen to be relatively thicker (~300 nm) than the

conventional practice to avoid any negative influence of the layer thickness on the device performance. Finally, PEDOT:PSS layer (~50 nm thick) was preheated at 90°C in an ethanol medium. Subsequently, it was spin-coated by adding a drop-wise 20 μL sample at 2000 rpm for 60 s on the P3HT:PCBM layer. The entire stack was dried at 120°C for 2 hr in argon atmosphere before taking the top contacts.

Cell B consists of only the ZnO nanorods (NRs) and organic counterparts. Direct growth of ZnO NRs was carried out hydrothermally on the ITO substrate, which was placed horizontally at the bottom of the Teflon-lined stainless steel autoclave. The working solution was prepared using a 30:10 mM aqueous mixture of zinc nitrate hexahydrate ($Zn(NO_3)_2 \cdot 6H_2O$) and hexamethylenetetramine (HMT, $C_6H_{12}N_4$) HMT served as a structure orienting agent toward the formation of ZnO NRs by chelation effect. The reaction was carried out for 1 hr at a temperature of 90°C. After completion of the reaction, the autoclave was cooled naturally to ambient temperature, ITO coated glasses were taken out and washed thoroughly with cold water and dried in a hot air oven at 120°C. Next, PCBM, P3HT:PCBM, and PEDOT:PSS were spin-coated on it followed by the same technique as mentioned for Cell A. In this case, as PCBM was coated on a vertically aligned NR array, most of it was soaked by the ZnO NR layer, and so, the actual thickness of this layer cannot be estimated correctly.

To fabricate Cell C, first, a dense ZnO layer with ~30 nm thickness was deposited on the cleaned ITO Substrate by radio frequency (RF) reactive sputtering. The ZnO (>99%) target was used for the deposition at an RF power of 150 W, temperature 270°C, chamber pressure 2.2×10^{-2} mBar, and duration 6 min. The deposition entails the use of 40:10 argon: oxygen as an RF gas mixture. Then ~25 nm thick ZnMgO layer was deposited on it using pulsed laser deposition (PLD) technique from a ceramic target containing ZnO:MgO at 90:10 wt% at a process temperature of 700°C. The second

harmonic of Nd:YAG laser, operated at a wavelength of 533 nm with a repetition rate of 10 Hz, and a pulse duration of 7 ns was used [286] for this purpose. The other organic counterparts of the cell were coated sequentially, followed by top contact formation similarly, as mentioned in the case of Cell A.

As can be seen from Fig.5.1, Cell D was composed of both ZnO/ZnMgO dense layer and ZnO NR array deposited on it. The ZnO/ZnMgO thick layer and ZnO NR array were deposited following the recipe as adopted for Cell C and Cell B, respectively. The other organic semiconductors were deposited as adopted for Cell A.

5.2.3. Characterization:

Philips PAN alytical X'Pert Pro x-ray diffractometer operated within 20 –80 degree scanning angle with Cu Kα x-radiation source (λ=1.540598 Å) was used to explore the crystalline properties of the deposited metal oxide layers. The morphological aspects of the deposited metal oxide layers were investigated using a Zeiss Sigma field-emission-scanning-electron-microscope (FESEM) UV– Vis Optical absorption spectrum was measured using a UV-Vis-NIR Spectrometer (Make-PerkinElmer, Model-Lambda 950, Serial Number-950L1103044). The current-voltage (I–V) measurements of the fabricated cells were carried out in the presence of light with the help of a source meter (B2912A, Agilent, U.S.A.), broadband light source (Science Tech, Canada), and a monochromator (Science Tech, Canada), using solar intensity 1000 W/m^2. PVE300 Photovoltaic EQE (IPCE) and I.Q.E. solution – Bentham (with an integrated sphere) was used to measure the quantum efficiency of the fabricated solar cells. Dielectric measurements were carried out with LCR Meter (NF Corporation, ZM 2376).

5.3. Result Analysis:

Morphological features of the individual layers of RF deposited ZnO, PLD deposited ZnMgO, and hydrothermally grown ZnO on ITO substrates are shown in Fig.5.2.

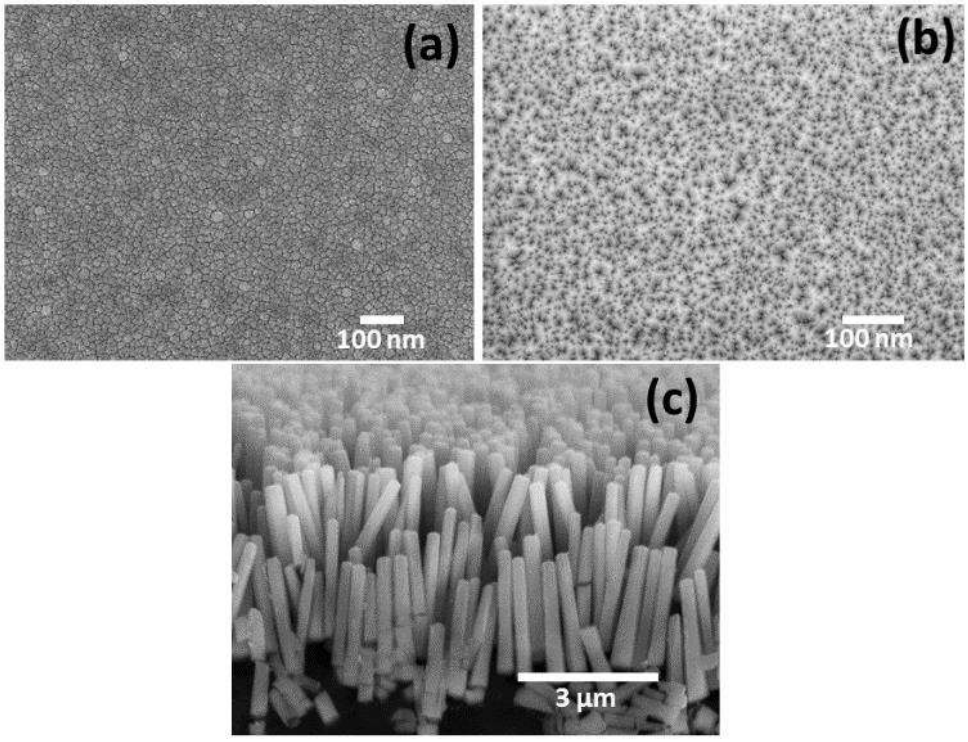

Fig.5.2. FESEM images showing the topography of (a) RF grown ZnO layer (b) PLD grown ZnMgO layer and (c) cross-sectional and topographical view of hydrothermally grown ZnO film with nanorod arrays.

The as-grown reactive RF sputtered ZnO film was found to be composed of densely packed grains with almost spherical (Fig.5.2a). The average grain diameter was found to be ~30 nm. The PLD grown ZnMgO layer showed further compactness of the surface composed of smaller particles (Fig.5.2b), however, the average grain diameter cannot be estimated from this image due to the non-distinguishable nature of the individual grains. On the other hand, the hydrothermally grown ZnO film revealed (Fig.5.2c) the formation of c-axis oriented hexagonal nanorods with about 3 µm in length and 150 nm in diameter. Good alignment and compactness of the nanorods in the matrix along with the high

surface-to-volume ratio of individual nanorods indicate its usefulness as an active layer in such inorganic-organic hybrid solar cells.

The x-ray diffraction (XRD) patterns of the metal oxide layers grown using three different techniques on ITO substrates are presented in Fig.5.3a. In this case, the signature diffraction peak for wurtzite (hexagonal) ZnO obtained from (002) diffraction plane at $2\theta = 34.42°$ (JCPDS # 361451) has been presented as a magnified view within a small angle ($2\theta = 32.0°$ to $37.0°$) to have a clear comparative idea about the crystalline structure of the deposited films. The (002) diffraction peak for reactive RF sputtered dense ZnO film was found to be centered at $2\theta = 34.44°$ with moderately broad full width at half maximum (FWHM). The diffraction peak was centered at the same position of 2θ for the hydrothermally grown ZnO layer; however, the peak was more intense than the RF ZnO with a small lowering in FWHM value. Interestingly, for the PLD-grown ZnMgO layer, the position of the (002) peak was found to be shifted slightly towards a lower 2θ value and was centered at 34.19°. This might be attributed to the generation of strain caused by either the substitution of Zn by Mg or the positioning of Mg in the interstitial ZnO lattice. The FWHM was also highest for this case, which is due to the lowering of crystallite size in PLD grown ZnMgO film, as is evident from the FESEM image (Fig.5.2b) also. Debye-Scherrer equation [crystallite size $D = (0.9\lambda/\beta\text{Cos}\theta)$, where, λ is the wavelength of x-radiation, i.e. 1.540598 Å in this case and β is the FWHM] was applied to calculate the crystallite size of RF deposited ZnO and PLD-deposited ZnMgO which yielded a value of about 40 nm and 10 nm, respectively for these two cases. The broader FWHM of ZnMgO and its shift toward lower 2θ values are attributed to smaller crystallite size, associated lattice strain ($8.66 \times 10\text{-}4$ for RF ZnO and $34.65 \times 10\text{-}4$ for ZnMgO) and decrease in ideal axial (c/a) ratio after Mg incorporation.

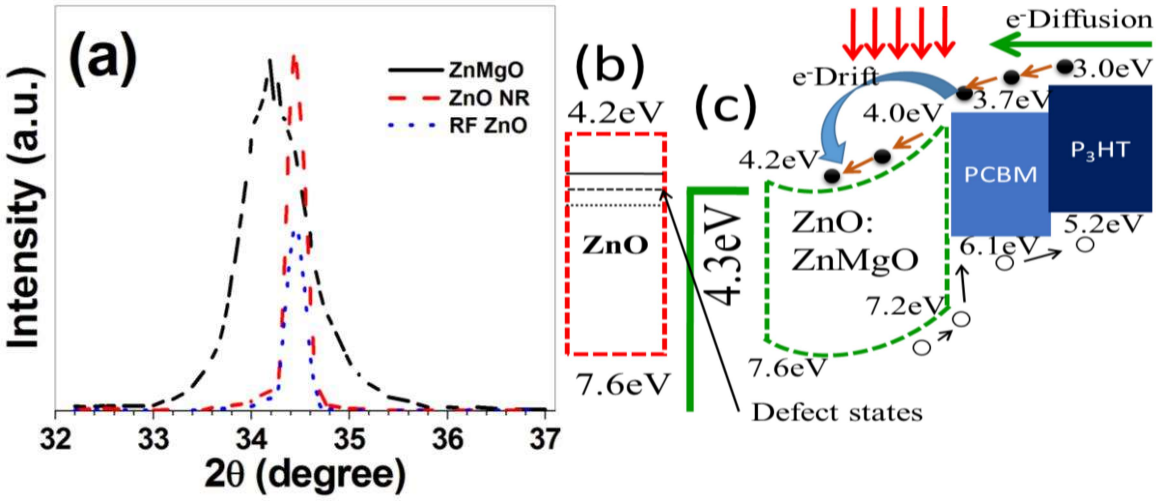

Fig.5.3. (a) XRD patterns for RF ZnO, PLD ZnMgO, and ZnO NR layers (b) ZnO layer with defect states and (c) band alignments across the solar cell structure representing light-induced passivation occurring at the Mg:ZnO/PCBM/P3HT:PCBM interface.

Defect states in ZnO and band alignment across the ZnO-ZnMgO/P3HT:PCBM are shown in Fig.3b and 3c, respectively. The defect states in ZnO are primarily due to oxygen vacancies in the as-grown sample. These defect levels act as carrier traps and lead to a reduction in cell performance. Another aspect being noted is the surface charge accumulations of photo-generated carriers, which are known to bring changes in VOC and conversion efficiency [289,290]. Annealing causes an increase in the crystallinity of P3HT and a lowering in the effective bandgap of the blend [289,290]. By introducing the PCBM layer and ZnO-ZnMgO dense layer, the junction electric field strength increases, this, in turn, reduces the charge accumulation at the surface. As a result, the open-circuit voltage of the solar cell decreases, which has further been elaborated by the capacitance-voltage (C–V) measurements.

The C–V characteristics of the ITO/ZnO/ZnMgO and ITO/ZnO NR electrodes are measured to compare their electrical properties regarding charge trapping and are shown in Fig.5.4. Fig.5.4a reveals an increase in capacitance for ITO/ZnO/ZnMgO electrode

than ITO/ZnO NR electrode. The exponential increase in capacitance leads to significant electron concentration near the cathode and hole accumulation near the anode [291].

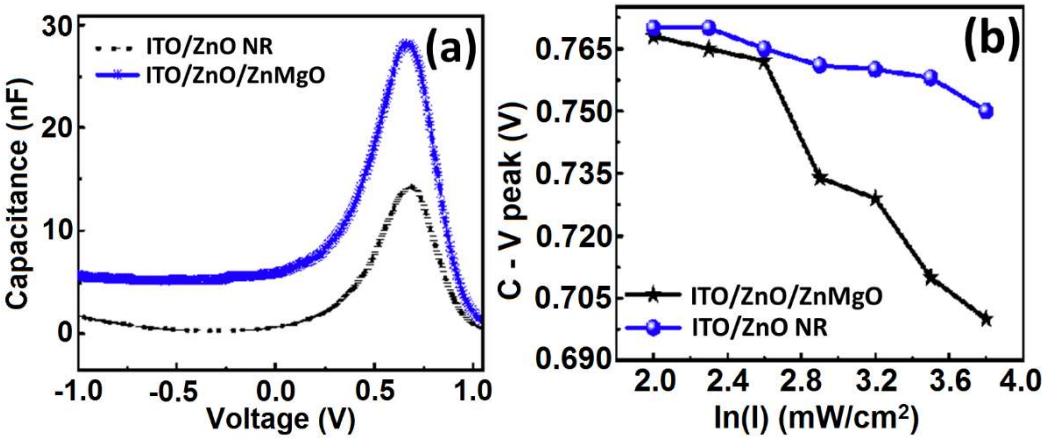

Fig.5.4 (a) C–V characteristics of ITO/ZnO NR and ITO/ZnO/ZnMgO electrodes and (b) C-V peak shift with variation in photoexcitation intensities on the ITO/ZnO NR and ITO/ZnO/ZnMgO electrode structures.

The calculated inherent electric field was found to be increased from 35 mV mW^{-1} cm^2 for ITO/ZnO NR electrode to 80 mV mW^{-1} cm^2 for ITO/ZnO/ZnMgO electrode. These values are indicating to better charge separation capabilities in the latter case. The C–V characteristic curve, which is used to investigate the effects of surface charge accumulation on VOC, shows peak shifts towards lower voltage values (Fig.4b) for the ITO/ZnO/ZnMgO electrode than the ITO/ZnO NR electrode on photo-irradiation. This is due to a decrease in effective potential barriers at the photovoltaic layer and ITO interface, which is correlated with improved current collection efficiencies. This, in turn, leads to improvements in short circuit current density, fill factor, and photovoltaic conversion efficiency.

To investigate the optical properties, UV−Vis absorption spectroscopy with ITO/P3HT:PCBM/PEDOT:PSS and ITO/ZnO/ZnMgO/P3HT:PCBM/PEDOT:PSS layers were carried out, and the corresponding spectra are presented in Fig.5.5. Two different absorption peaks centered at ~335 and ~511 nm are observed (Fig.5.5a) for the cell configuration with pure organic layers. These peaks correspond to fullerene (C60)

derivatives and polythiophene [292] present in the P3HT:PCBM/PEDOT:PSS layers. Significant improvement of absorption, both in terms of intensity and shifting toward the visible region, has been achieved after incorporating ZnO/ZnMgO dense layer in the electrode structure, as can be seen from curve b of Fig.5.5. A redshift to 545 nm was attained for the peak, which was earlier centered at 507 nm. The total absorption also increases after incorporating ZnO/ZnMgO dense layer, as can be seen from the enhanced area under the curves in Fig.5.5b. Though it is not the exact measure of total photon energy, however, a gross idea can be obtained about the increment in absorption after incorporating the metal oxide layers. About 38.67% (from 188.34 to 261.18 for Fig.5.5a and Fig.5.5b, respectively) increase in absorption was found. The increase in absorption is caused by the evanescent electromagnetic waves owing to the presence of ZnO/ZnMgO dense and thin layers [293,294].

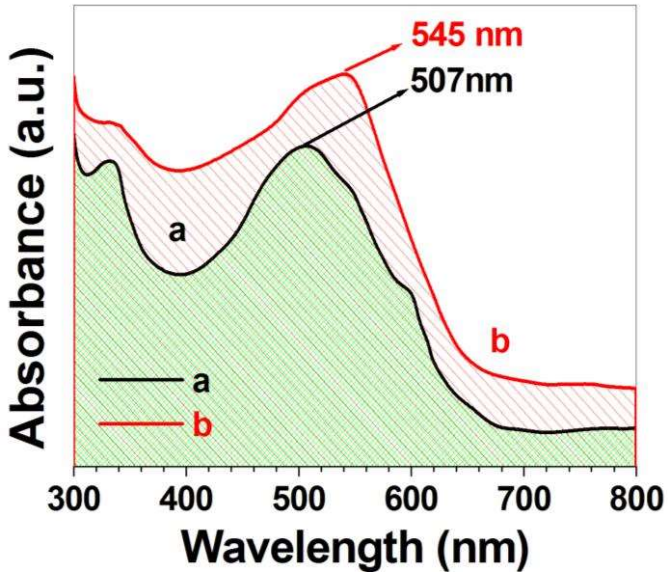

Fig.5.5. Optical absorption spectra of (a) PEDOT:PSS/P3HT:PCBM and (b) ZnO/ZnMgO/P3HT:PCBM/PEDOT:PSS layers deposited on ITO.

Now, the performance of the four different types of fabricated cells viz. Cell A, Cell B, Cell C, and Cell D has been measured, and the current density–voltage (J–V) curves are presented in Fig.5.6, and the cell parameters are shown in Table 5.1.

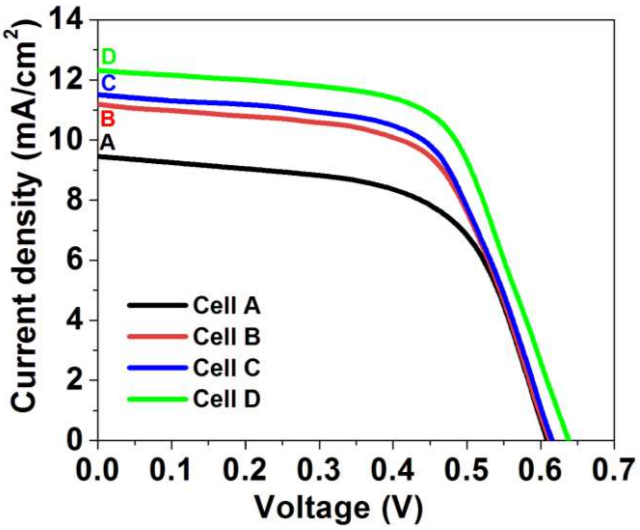

Fig.5.6: J – V curves of the four different inverted cells fabricated in this work.

Table 5.1: Cell parameters of the four different fabricated cells

Cell	J_{SC} (mA/cm^2)	V_{OC} (mV)	FF (%)	η (%)
Cell A	9.5	610	60.5	3.50
Cell B	11.2	613	61.4	4.21
Cell C	11.5	619	61.8	4.39
Cell D	12.3	640	63.0	4.95

Significant and gradual increment in J_{SC} has been observed from Cell A to Cell D. This improvement may be attributed to better carrier generation and collection properties achieved by the application of the ZnO/ZnMgO barrier cum electron selective layer. The latter inhibits unwanted carrier recombination in the bulk heterostructure. The properties improved further on the application of ZnO NRs in association with the dense layer. The best performance has been attained by Cell D ($\eta = 4.95\%$), which is better than many recent reports on IOSCs fabricated using bulk heterojunctions [291]. The ZnO NR arrays in Cell B helps to achieve better adsorption than that of the polymeric counterparts. This is because of the high surface-to-volume ratio of the NRs than the pure planner structure as in Cell A. As the organic counterparts of the cell are now having a higher exposed surface area and ZnO NRs are effectively increasing the optical path length, photon absorption followed by carrier generation will also be higher for the case of Cell

B. The presence of ZnO NRs also facilitates carrier separation owing to the electric field generated between PCBM and ZnO NR, followed by charge migration to the ITO electrode through the NRs. An enhancement of Jsc reflects this in Cell B (11.2 mA/cm^2) than in Cell A (9.5 mA/cm^2).

For the case of only ZnO/ZnMgO dense layer coated ITO electrode (Cell C), the surface-to-volume ratio is lower than that in Cell B, but the field strength increases significantly. The measured C–V characteristics have revealed this. This increased field strength compensates for the loss in active surface area. Finally, it results in some increment in both J_{SC} and V_{OC} than both Cell A and Cell B. This is also supported by the better light absorption capability of the ZnO/ZnMgO supported polymeric layers. When a combination of both ZnO/ZnMgO dense layer and ZnO NR was chosen to act as the active layer as per schematic of Cell D, notable increments in J_{SC}, V_{OC}, FF, and efficiency were observed. This could be attributed to the better electrical and optical property exerted by the active metal oxide layers where the dense layer exerts the required field for charge separation. The NR layer provides a higher exposed surface area for polymer adsorption, followed by carrier collection. A notable improvement in V_{OC} and fill factor can be attributed to the excellent material property realized after incorporating the ZnO/ZnMgO barrier cum electron selective layer. As can be seen from the electronic band structure of the device (Fig.4.3b, 4.3c), the presence of a thin ZnMgO layer between P3HT:PCBM and dense ZnO layer suppress the impact of oxygen vacancies which in turn improves the charge carrier mobility and lowers the leakage current. In this work, the use of a blend of P3HT:PCBM despite only P3HT (which is used conventionally) with a higher thickness (~300 nm) puts some positive impact in improving photon absorption and drift current. The drift current and resistance values are enhanced in Cell D through a substantial reduction in the interface states and trap states of ZnO and

ZnO/ZnMgO/organic (P3HT:PCBM/PCBM) interfaces. The best performing cell (Cell D) showed shunt and series resistance of 30×10^5 ohm and 0.2 ohm, respectively.

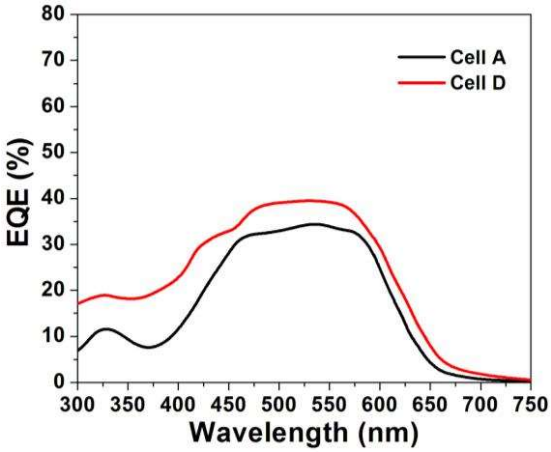

Fig.5.7. EQE plots for Cell A and Cell D.

A comparison of J_{SC}, V_{OC}, FF and efficiency (η) of some recent reports on P3HT:PCBM based organic heterojunction solar cells are shown in Table 5.2.

Table 5.2:Comparison of cell parameters with other reports

Cell configuration	F.F. (%)	Jsc (mA/cm2)	VOC (mV)	η (%)
P3HT:PCBM/PEDOT:PSS [295]	68.50	10.06	615	4.24
ZnO/ P3HT:PCBM [296]	36.00	12.55	560	2.51
PEDOT:PSS(DMF)\P3HT:PCBM: ZnO [297]	49.28	11.91	579	3.39
P3HT:PCBM/PEDOT:PSS [293]	57.60	13.3	629	4.82
ZnO/ZnMgO/ZnO NR/P3HT:PCBM (Present work)	63.00	12.3	640	4.95

External quantum efficiency (EQE) has been measured for Cell A and Cell D, which is presented in Fig.5.7. A notable amount of enhancement in EQE has been observed for Cell D than Cell A over the entire scanned wavelength region. However, a significant increment was found within short to mid-wavelengths, i.e., within 300 to 550 nm. This, in turn, refers to the usefulness of incorporating the barrier layer and NR-based absorber layer in the BHJ IOSC architecture.

5.4 Device Reliability:

The cells fabricated in this case by incorporating the barrier layer and nanorod architecture i.e. Cell B, Cell C, and Cell D were subjected to reliability study by soaking light for 1400 hours at 55°C and 60% relative humidity. The variation in normalized efficiency (%) concerning light soaking duration for these three cells is presented in Fig.5.8.

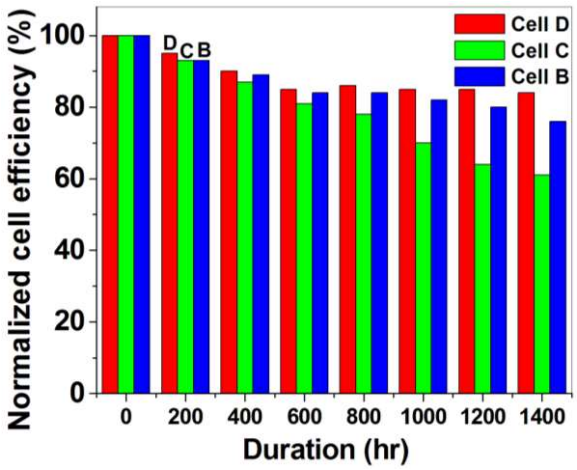

Fig.5.8. The plot of normalized efficiency for Cell B, Cell C and Cell D with respect to light soaking duration.

In this case, the normalized efficiency values for Cells B, C, and D were found to be degraded to 76%, 61%, and 84% after 1400 hrs of light soaking. The degradation in the value of efficiency was least for Cell D, which could be attributed to the presence of both the barrier layer and NR architecture in this particular cell configuration. The high surface-to-volume ratio and dense packing of such ZnO NR array are responsible for better adsorption by the polymers and protect them from environmental exposure. The performance of an organic solar cell mainly deteriorates due to surface degradation, which in turn affects the junction field strength. Due to the introduction of the barrier layer and structural modifications made in this case, Cell D showed significantly better stability

than Cell B and Cell C. P3HT tends to get photo-oxidized rather quickly in ambient conditions; however, the addition of PCBM [299] and partial encapsulation within ZnO NR array considerably slow down this degradation process. Under illumination and oxygen-rich environment, P3HT is converted to metastable P3HT+-O2- complex, which results in trap states that reduce carrier transport and mobility [300-302]. The use of thicker (~300 nm) P3HT:PCBM layer and deliberate introduction of thin PCBM layer (~100 nm) in this case can reduce such trap states notably. The ZnMgO layer between P3HT:PCBM and dense ZnO layer suppresses the impact of oxygen vacancies, which in turn improves the carrier mobility and lowers leakage current in Cell D. If any of these layers, viz. either the barrier layer or the NR layer is absent, i.e., for the case of Cell B and Cell C, respectively, the combined effect of charge separation and dye adsorption cum environmental protection would not be available. As Cell C does not contain any NR structure, the polymer blend P3HT:PCBM remains more exposed to the environment than Cell B. This might be one of the reasons behind the maximum degradation that was faced by Cell C with time. Cell D exhibits the best efficiency and stability in the present study. It also outperforms many of the reported contemporary devices.

5.4. Chapter Conclusion

The inverted organic solar cells on ITO substrates were fabricated with and without using the ZnO/ZnMgO barrier cum electron selective layer and ZnO NR array as the absorbing layer. The cells with four different structures were fabricated and examined. The use of the ZnMgO layer between P3HT:PCBM and dense ZnO layer have been found to suppress the impact of oxygen vacancies, which in turn improves the charge carrier mobility and lowers leakage current. The total current and stability were enhanced through the application of three different junctions and corresponding layers. The stability

of the device and diffusion current was improved by using P3HT:PCBM/PEDOT:PSS junction, where the PCBM layer (~100 nm) protects the thick and active P3HT:PCBM layer (~300 nm). Drift current was improved through the modification of ZnO layer-based junction, i.e., ZnO/ZnMgO heterojunction. Presence of a thick (~300 nm) P3HT:PCBM (1:1) layer instead of the usual and only P3HT layer was responsible for improving the carrier collection efficiency. Incorporation of ZnO NR layer enhances polymer adsorption, carrier collection and protects the polymers from environmental exposure owing to its high surface-to-volume ratio and compact distribution. Best photoconversion efficiency of 4.95% significant reliability after 1400 hrs of light soaking was observed for Cell D, which was composed of both barrier layer and NR structure. This report is likely to motivate future work toward further improvement of cell parameters using this cell architectural concept.